Supplementary Information

Supplementary Experimental Procedures:

Cell lines: MPNST cell lines utilized for our studies included the NF1-associated: ST88-14 (provided by Dr Jonathan Fletcher, Brigham and Women's Hospital, Boston, MA), T265 (provided by Dr George De Vries, Hines VA Hospital, Hines, IL), S462 (provided by Dr Brian Rubin, Cleveland Clinic, Cleveland, OH) and the MPNST642 isolated in our laboratory (see below) and the sporadic MPNST cell lines: STS26T (provided by Dr Steven Porcelli, Albert Einstein College of Medicine, Bronx, NY) and MPNST724 (provided by Dr Jonathan Fletcher) and were propagated and maintained as previously described (Miller SJ, et al. Cancer Res 2006;66:2584-91). Primary human adult Schwann cell cultures established from human cauda equina nerves were provided by Dr Patrick Wood (Miami Project, University of Miami, Miami, FL) and maintained as previously described (Casella GT, et al. Glia, 2000;30:165–177).

.

MPNST642 Isolation This procedure was conducted with approval from the Institutional Review Board at The University of Texas M. D. Anderson Cancer Center and informed consent from the patient. Tumor cell isolation was conducted as commonly described. Briefly, fresh sterile samples from surgically resected tumors were minced in culture medium and then digested via incubation with collagenase type I (3%), DNase I (0.02%), and hyaluronidase (1.5 mg/ml) at 37°C for 2-4 h. The sample was strained through a wire mesh screen, and undigested tissue was discarded. After centrifugation, washes, and resuspension in PBS, the sample was gently transferred to Histopaque tubes containing 10 ml Histopaque (100%; Sigma) overlayed with 15 ml of Histopaque (75%). The tubes were then centrifuged at 40°C for 30 min at 1200g. After centrifugation, the

tumor cells located in the top interface (over the 75% Ficoll were collected and plated. Cells were cultured and passaged in DMEM containing 10% FBS (Life Technologies).

Short tandem repeat (STR) DNA fingerprinting

DNA was extracted from all MPNST cell lines and from the original human tumor from which MPNST642 was isolated using the Qiagen Blood & Cell Culture DNA Maxi kit according to the manufacturer's protocol (Qiagen, Valencia, CA). DNA fingerprints were obtained using the AmpFlSTR Identifier PCR Amplification kit (Applied Biosystems, Foster City, CA) according to the manufacturer's protocol. The kit amplifies the amelogenin gender-determining marker and 15 tetranucleotide repeat loci in a single PCR amplification using 33 primers (the extra one is a degenerate primer targeting a mutation at the D8S1179 locus). That combination of markers is consistent with worldwide database recommendations for identity testing. Each of the STRs used in this study has a tetranucleotide repeat sequence. Allele calls were made from peak plots by comparing peaks to known fragment sizes using GeneMapper 4.0 (Applied Biosystems).

Cell growth assays

MTS assays: these were conducted using CellTiter96 Aqueous Non-Radioactive Cell Proliferation Assay kit (Promega Corp, Madison, WI), per manufacturer's instructions. Drugs were administered at doses and for intervals as indicated. Absorbance was measured at a wavelength of 490 nm, and the absorbance values of treated cells are presented as a percentage of the absorbance of untreated cells. Drug concentrations required to inhibit cell growth by 50% (GI_{50}) were determined by interpolation of dose-response curves. Colony formation assay: MPNST cells were pre-treated in culture dishes with drugs at concentrations and intervals as indicated. One hundred viable cells per well were re-plated and allowed to grow in normal medium for 10 days and then

stained for 30 min at room temperature with a 6% glutaraldehyde, 0.5% crystal violet solution. Pictures were captured digitally and colonies were counted. Anchorage independent growth: MPNST 642 ($1x10^3$ viable cells) were plated in a 24-well plate in culture medium containing 0.35% agarose overlying a 0.7% agarose layer. Cells were incubated for 3 weeks at 37°C. Cells were stained with *p*-iodonitrotetrazolium violet (1mg/ml) for 24h at 37°. Number of colonies per well were counted. All experiments were repeated at a minimum three times for each cell line.

Apoptosis assays

Apoptosis was measured using the Apoptosis Detection kit I (BD Biosciences, San Jose, CA) per manufacturer's recommendations. As a standard, $1x10^6$/mL of cells per treatment condition (time and dose as indicated) were fixed and stained with 5 µL Annexin V–FITC (BD PharMingen, San Diego, CA) and 5 µL propidium iodide (Sigma, St Louis, MO). Flow cytometric analysis was performed for $1X10^4$ cells and analyzed by FACScan (Becton Dickinson, Franklin Lakes, NJ) using a single laser emitting excitation light at 488 nm. Data were analyzed by CellQuest software (Becton Dickson, Franklin Lakes, NJ).

Transfection procedures: siRNAs (pools targeting: beclin, ATG5, ATG7, IRGM, p53, and control non-targeting constructs) were introduced into cells using Lipofectamine 2000 (Invitrogen, Carlsbad, CA) per manufacturer's instructions. Briefly, $2x10^5$ cells were plated in each well of a six-well plate and incubated overnight. A mixture of siRNA (20 nM) and Lipofectamine 2000 diluted in Dulbecco's modified Eagle medium (DMEM) was added for 24 hr, followed by incubation in regular medium. Cells were harvested at indicated time points for specific experiments.

p53 sequencing

DNA sequencing of the *p53* gene (exons 4 to 9) was conducted as we have previously described (Das P, et al. Cancer, 2007: 6; 2323-33)

p53 transfection

Adp53 and AdLacZ adenoviruses were produced and titered by the Vector Core Laboratory at M.D. Anderson Cancer Center. Transfection procedures were conducted as we have previously described (Liu J, et al. MCT, 2006: 4;803-10).

RT-PCR and qRTPCR

These experiments were conducted as we have previously described (Jin Z, et al. CCR, 2008: 14;5033-42). Primers used are depicted in the table below:

Gene name	Forward primer	Reverse primer
ATG5	TGGGGTGGATATAGGGCATA	GACCTGGAGCCAATGAAAAA
ATG7	ACCCAGAAGAAGCTGAACGA	CTCATTTGCTGCTTGTTCCA
GAPDH	GAAGGTGAAGGTCGGAGTC	GAAGATGGTGATGGGATTTC
IRGM	CCCTTCGAAACACAGGACAT	AGTTCTCCAGGGTTGTGGTG
CXCR4	GGTGGTCTATGTTGGCGTCT	TGGAGTGTGACAGCTTGGAG
TMEM74	TGACCAGGCAGATACAGCAG	GTGGAGAAGTCCTGGTGGAA
NFKB1	CCTGGATGACTCTTGGGAAA	TCAGCCAGCTGTTTCATGTC

Quantification of acidic vesicular organelles

Assays were conducted as we have previously described (Zou CY, et al. MCT, 2009: Epub ahead of print).

Electron Microscopy

STS26T and MPNST724 cells were grown on glass coverslips and treated with PCI-24781 (1μM) or DMSO alone for 24, 48, or 72 hours and then fixed for one hour with a solution containing 3% glutaraldehyde plus 2% paraformaldehyde in 0.1 M cacodylate buffer (pH 7.3). After fixation, the samples were post-fixed in 1% OsO_4 in the same buffer for 30min then stained with 1% uranyl acetate. Representative areas were chosen for ultrathin sectioning and electron microscopic viewing (JEM 1010 transmission electron microscope; JEOL, Peabody, MA), as previously described (Takeuchi H, et al. *Cancer Res* 2005:65;3336–46). Digital images were also obtained (AMT imaging system; Advanced Microscopy Techniques Corp., Danvers, MA). Three replicates were performed for each experiment.

Autophagy associated Western blot analyses interpretation related information

Conversion of soluble LC3-I to lipid bound LC3-II is associated with the formation of autophagosomes. Cleavage of LC3 at the carboxy terminus immediately following synthesis yields the cytosolic LC3-I form. During autophagy, LC3-I is converted to LC3-II through lipidation by a ubiquitin-like system involving Atg7 and Atg3 that allows LC3 to become associated with autophagic vesicles. The presence of LC3 in autophagosomes and the conversion of LC3 to the lower migrating form LC3-II have been used as indicators of autophagy. WB for LC3 demonstrating enhanced expression of LC3B-II (normalized to actin) is an indicator of increased number of autophagosomes. The inhibitors chloroquine and bafilomycin block the last stages of productive autophagy thus will result in autophagosome accumulation; WB for LC3B-II in the presence of these inhibitors is expected to show increased LC3B-II levels (normalized to actin). Combining chloroquine or bafilomycin with compounds that enhance productive autophagy is

expected to show further increase in LC3B-II expression. Cells stably transduced with LC3-GFP can be used to evaluate impact of a investigated compound on productive autophagy. When GFP-LC3 is delivered to a lysosome the LC3 part of the chimera is sensitive to degradation, whereas the GFP protein is relatively resistant to hydrolysis. Therefore, the appearance of free GFP on WB (blotted for GFP) can be used to monitor lysis of the inner autophagosome membrane and breakdown of the cargo. For more detailed information please refer to: "Guidelines for the use and interpretation of assays for monitoring autophagy in higher eukaryotes" (Klionsky et al. Autophagy, 2008: 2;151-75).

Focused Autophagy PCR array

Total RNA was isolated from MPNST724 and STS26T cells (PCI-24781 treated [0.5μM/24h] and untreated) using Trizol Reagent (Invitrogen, Carlsbad, CA). After DNase treatment, RNA was further cleaned up using Qiagen RNeasy® Mini Kit (Qiagen, Valencia, CA). cDNA was synthesized by RT2 First Strand kit (SABiosciences, Frederick, MD) following manufacturer's instructions. Gene expression profiling using the Autophagy RT^2 Profiler™ PCR Array (SABiosciences, Frederick, MD) was conducted. This platform is designed to profile the expression of 84 key genes involved in autophagy (for a comprehensive list of included genes see *www.sabiosciences.com*). qRTPCR was conducted using Mastercycler Epgradients realplex (Eppendorf AG, Hamburg, Germany) based on array manufacturer's instructions. Relative gene expression was determined using the ΔΔCT method. Data were further analyzed by PCR Array Data Analysis Web Portal (*www.SABiosciences.com/pcrarraydataanalysis.php*). All experiments were repeated thrice.

In vivo animal models

All animal procedures and care were approved by the MD Anderson Cancer Center Institutional Animal Care and Usage Committee. Animals received humane care as per the Animal Welfare Act and the NIH "Guide for the Care and Use of Laboratory Animals." For experiments evaluating effect of treatment on local tumor growth trypan blue staining confirmed viable MPNST cells (MPNST642, MPNST724 [MPNST724 stably transduced to express LC3-GFP was used to evaluate effect of therapy on GFP cleavage], and STS26T; 1-2 x 10^6/0.1 mL HBSS/mouse) were used. Cell suspensions were injected subcutaneously into the flank of six week old female hairless SCID mice (*n* = 10/treatment group) and growth was measured twice weekly; after establishment of palpable lesions (average diameter >5mm) mice were assigned to treatment groups as described below. An experimental lung metastasis MPNST model was used to evaluate metastases' growth. STS26T cells (1 x 10^6/0.1 mL HBSS/mouse) were injected into the tail vein of female SCID mice. Ten days after injection (a time-point by which 95-100% of mice develop established lung metastases) mice were allocated to treatment groups as per below. Therapeutic regimens included a two arm study: 1) control - DMSO vs. 2) PCI-24781 (25mg/kg/d or 50mg/kg/d for five days/week) and a four armed study: 1) DMSO; 2) PCI-24781 (25mg/kg/d for five days/week); 3) chloroquine (50mg/kg/d for five days a week); and, 4) combination of PCI-24781 and chloroquine (doses and schedule as above). In the latter studies, including a chloroquine arm, this drug was initiated a day prior to PCI-24781 treatment. Mice were followed for tumor size, well being, and body weight and sacrificed when control group tumors reached an average of 1.5 cm in their largest dimension. Tumors were resected, weighed, and frozen or fixed in formalin and paraffin-embedded for immunohistochemical studies. For lung metastasis studies mice were followed for body weight and well being and sacrificed after two weeks of treatment. Lungs were resected, evaluated macroscopically for tumor load and weighed.

Immunohistochemistry and TUNEL assays

Immunohistochemistry and TUNEL assays were performed as previously described (Lopez G, et al. CCR, 2009: 15; 3472-83) .

Supplementary Tables:

Table S1 – Deregulated genes in response to PCI-24781 treatment based on a focused Autophagy PCR microarray

		Fold change		
Name	**Accession No.**	**STS26T**	**MPNST724**	**Relevant Ref.**
Upregulated				
IRGM	XR_040407	36 (±2.3)	38 (±1.7)	1
TMEM74	NM_153015	7.5 (±1.9)	33 (±11)	2
CXCR4	NM_003467	16 (±2.3)	32 (±5.3)	3
ATG4A	NM_052936	3 (±0.6)	29 (±8)	4
Downregulated				
PIK3CG	NM_002649	-7 (±2.9)	-8 (± 2.1)	5
FAS	NM_000043	-4 (±0.2)	-10 (±3.3)	6
NFKB1	NM_003998	-5.5 (±0.03)	-13 (±2.8)	7
CDKN1B	NM_004064	-4 (±1.5)	-9 (±4)	8
RGS19	NM_005873	-3.3 (±1.3)	-21 (±11)	9

1. Singh, S.B., Davis, A.S., Taylor, G.A., Deretic, V. (2006). Human IRGM induces autophagy to eliminate intracellular mycobacteria. Science *313,* 1438-41.

IRGM (immunity-related GTPase family, M.) belongs to the immunity-related guanosine triphosphatases family, also known as p47 GTPases. Human IRGM, unlike its murine ortholog, is constitutively active and does not require IFN-γ for the induction of autophagy and it is thought to play a major role in innate immunity against intracellular pathogens. Genomewide association studies have demonstrated a contribution of IRGM variants to Crohn's disease (CD) susceptibility. Furthermore, non-coding single nucleotide polymorphism (SNP) variants in the IRGM locus were shown to be associated with an increased risk for CD. The first evidence indicating human IRGM is a functional protein was derived from a study demonstrating its association with the autophagy-targeted destruction of Mycobacterium bovis, BCG. IRGM inhibition was found to blocks starvation- and rapamycin-induced autophagy

2. Yu C, Wang L, Lv B, Lu Y, Zeng L, Chen Y, Ma D, Shi T, Wang L. (2008). TMEM74, a lysosome and autophagosome protein, regulates autophagy. Biochem Biophys Res Commun *369,* 622-29.

TMEM74 (Transmembrane protein 74) is a novel autophagy-related molecule shown to localize to lysosomes and autophagosomes. Overexpression of TMEM74 in HeLa cells resulted in autophagic vacuolization, increased the dotted distribution of MDC and GFP-LC3, and endogenous LC3-II levels. Wortmannin, an autophagy inhibitor, partially attenuated these effects. Moreover, knockdown of TMEM74 by siRNA abolished the autophagic characteristics induced by starvation. These findings demonstrate that TMEM74 may be involved in promoting functional autophagy during cell starvation and other stress conditions.

3. Levine B, Sodora DL. (2006). HIV and CXCR4 in a kiss of autophagic death. J Clin Invest *116,* 2078-80.

CXCR4 is the receptor for the CXC chemokine, SDF1. CXCR4 has been shown to play major physiological roles in embryogenesis, immunological surveillance, and lymphocyte trafficking. CXCR4 has been widely studied for it potential role in cancer progression and metastasis. Recently a role in autophagy has been demonstrated in the context of HIV infection. HIV envelope glycoprotein was found to induce CXCR4-dependent autophagy

in uninfected lymphocytes, required for both caspase-dependent, apoptotic cell death and caspase-independent, nonapoptotic cell death.

4. Mariño G, Uría J.A., Puente X.S., Quesada V, Bordallo J, López-Otín C. (2003). Human autophagins, a family of cysteine proteinases potentially implicated in cell degradation by autophagy. J Bio Chem *278,* 3671-78.

5. Miller S, Tavshanjian B, Oleksy A, Perisic O, Houseman B.T., Shokat K.M., Williams R.L. (2010) Shaping development of autophagy inhibitors with the structure of the lipid kinase Vps34. Science *327*, 1638-42.

6. Zhang Y, Wu Y, Cheng Y, Zhao Z, Tashiro S, Onodera S, Ikejima T. (2008). Fas-mediated autophagy requires JNK activation in HeLa cells. Biochem Biophys Res Commun *377,* 1205-10.

7. Djavaheri-Mergny M, Amelotti M, Mathieu J, Besançon F, Bauvy C, Souquère S, Pierron G, Codogno P. (2006). NF-kB activation represses tumor necrosis factor-a-induced autophagy. J Biol Chem *281*, 30373-82.

8. Liang J, Shao SH, Xu ZX, Hennessy B, Ding Z, Larrea M, Kondo S, Dumont DJ, Gutterman JU, Walker CL, Slingerland JM, Mills GB. (2007). The energy sensing LKB1-AMPK pathway regulates p27(kip1) phosphorylation mediating the decision to enter autophagy or apoptosis. Nat Cell Biol *9*, 218-24.

9. Ogier-Denis E, Petiot A, Bauvy C, Codogno P. (1997). Control of the Expression and Activity of the Gα-interacting Protein (GAIP) in Human Intestinal Cells. J Biol Chem *272*, 24599-603.

Supplementary Results:

- MPNST doubling times were calculated based on cell number counts at 24h time increments and were found to be as follows: S462 and STS26T ~16h, ST88 and MPNST724 ~24h, T265 ~28h, and MPNST642 ~48h.
- HDACis have been shown to exert anti-tumor effects through acetylation and activation of wild type p53 and p53 deregulation is a common event in MPNST. Therefore, we evaluated whether the growth-inhibitory effects of HDACi effects were linked to the p53 mutational status of the cells. Confirming and expanding previous data, p53 sequencing (exon 4-9) demonstrated p53 to be wild type in ST88, T265, and MPNST642 cells; p53 mutations were identified in S462 and MPNST724 cells (R110P and 254-d, respectively), STS26T cells were p53 null. These findings were further re-affirmed by corresponding p53 protein expression levels (WB; **Fig S2A**). Overall the most sensitive and most resistant MPNST cell lines harbor p53 mutations, indicating that HDACi response is independent of p53 mutation/function. To further evaluate whether functional p53 can modify MPNST-associated HDACi response, p53 was knocked down in ST88 cells (WTp53) and overexpressed in STS26T (p53 null), and cells were further treated with PCI-24781. As depicted (**Figure S2A**), p53 knockdown or overexpression did not affect HDACi-induced anti-MPNST pro-apoptotic effects.

Supplementary Figures

Supplementary Figure 1:

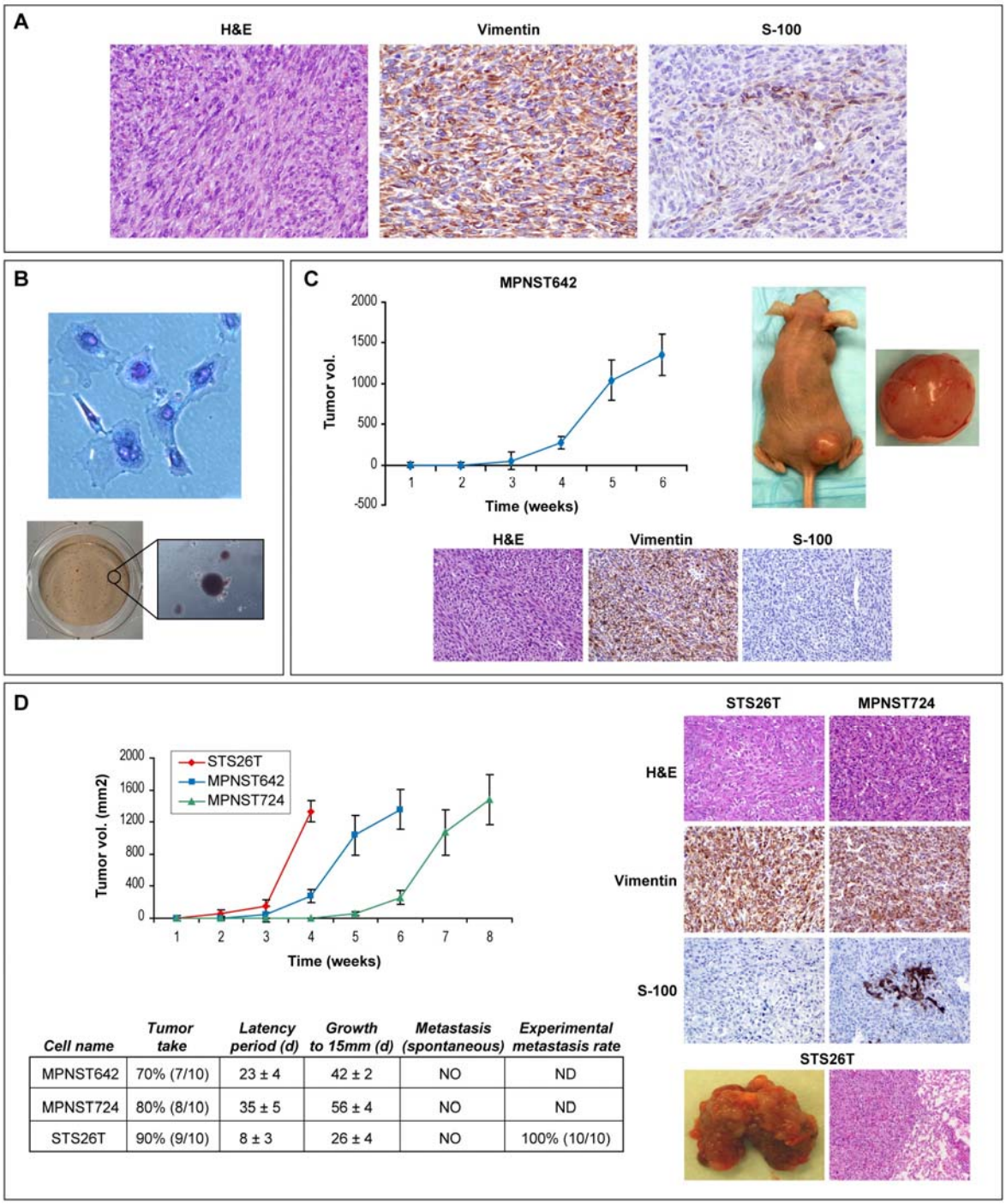

Cell name	Tumor take	Latency period (d)	Growth to 15mm (d)	Metastasis (spontaneous)	Experimental metastasis rate
MPNST642	70% (7/10)	23 ± 4	42 ± 2	NO	ND
MPNST724	80% (8/10)	35 ± 5	56 ± 4	NO	ND
STS26T	90% (9/10)	8 ± 3	26 ± 4	NO	100% (10/10)

Figure S1: MPNST cell lines. *A.* The cell line termed MPNST642 originated from a recurrent MPNST located in the forearm of a 21 year old male diagnosed with NF1 at childhood. Post-surgery, accelerated disease progression occurred and the patient

succumbed to extensive pulmonary metastatic disease within several months. Immunohistochemical stains of original tumor are depicted (X200); H+E demonstrating the histomorphology of the tumor which stained positively for vimentin and focally for S100; *B.* MPNST642 cells have been growing in culture continuously for >60 passages (morphology is depicted, Geimsa staining, upper panel) and they exhibit anchorage independent growth (lower panel). DNA fingerprinting confirmed the cell origin to be from the human tumor and demonstrated that no cross contamination has occurred in culture; *C.* MPNST642 cells ($2x10^6$/mouse, subcutaneous injection) grow as xenografts in SCID mice: graph demonstrates growth rate (see also table below), histomorphology is similar to that of original patient tumor although S100 staining is negative (loss of S100 expression is known to occur with MPNST progression); *D.* Two additional MPNST cell lines of those used in our study (STS26T and MPNST724; $1\text{-}2X10^6$/mouse) exhibit subcutaneous xenograft growth in hairless SCID mice. Growth curves of all three available xenografts are shown together to enable comparison (left upper panel). H+E and IHC staining of xenografts are depicted (right upper panel) STS26T xenografts are negative for S100 while MPNST724 are focally positive. In addition, tail vein injection of STS26T ($1X10^6$/mouse) results in reproducible lung metastasis – macroscopic and microscopic photographs are shown. The table summarizes the xenograft growth characteristics of all three human cell lines. STS26T are commonly used as a cellular model of sporadic MPNST and are widely accepted as a representative of this disease. MPNST724 have been kindly provided by Dr Jonathan Fletcher, the original diagnosis was made by a vastly experienced pathology team; S100 positivity in MPNST724 xenografts further supports the MPNST origin of these cells.

Supplementary Figure 2:

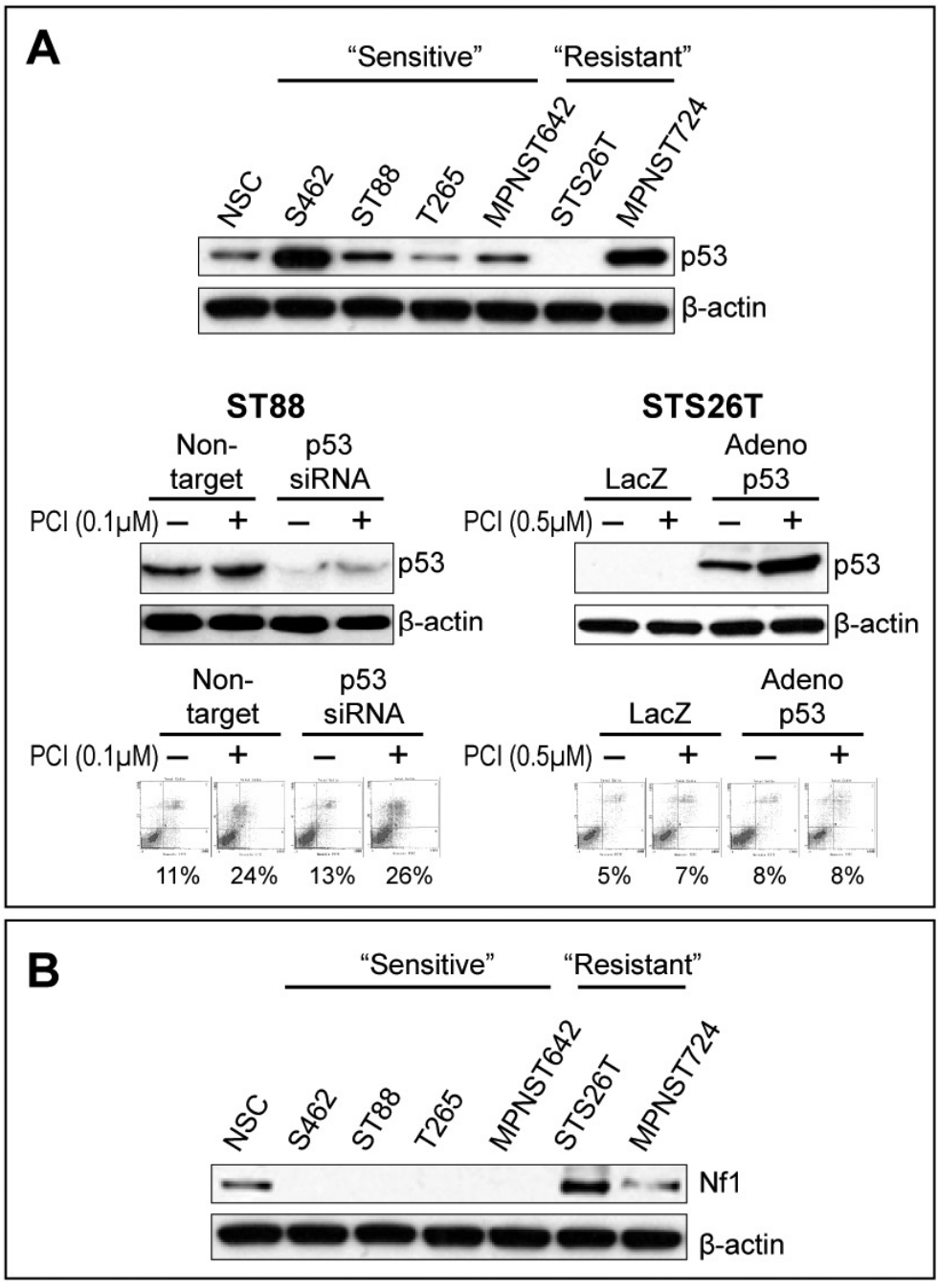

Figure S2: NF1 associated MPNST cells are highly sensitive to HDACi; sensitivity is independent of *p53* mutational status. *A.* Previous studies have identified S462 to harbor a *p53* mutation, STS26T was found to be *p53* null, and ST88 and T265 were shown to exhibit wild type *p53*. We have further sequenced MPNST642 (wild type) and

MPNST724 (mutated). WB analysis depicting p53 protein expression levels confirming with mutational status. Thus both the most HDACi sensitive (S462) and resistant (MPNST724) harbor *p53* mutations. Furthermore, *p53* siRNA knockdown in cells harboring the wild type gene (ST88) did not confer HDACi resistance and transient *p53* over-expression in null cells (STS26T) via adeno-p53 transfection did not enhance HDACi sensitivity in these resistant cells; *B.* All HDACi sensitive cells in our study were found to be NF1 associated (WB depicting loss of neurofibromin [Nf1] protein expression) while resistant cells were of sporadic MPNST origin, expressing Nf1. (NSC = normal human Schwann cells). Nf1 loss is the hallmark of NF1-associated MPNST. Several studies have identified somatic *NF1* mutations to occur in a subset of sporadic MPNSTs, although not uniformly in all cases (e.g. Bottillo et al. J Path, 2009: 217; 693-710). The exact prevalence and importance of Nf1 loss in sporadic MPNST tumorigenesis is currently unknown. Both sporadic MPNST cell lines used in our study, to the best of our knowledge the only ones currently available for testing, do express Nf1 protein.

Supplementary Figure 3:

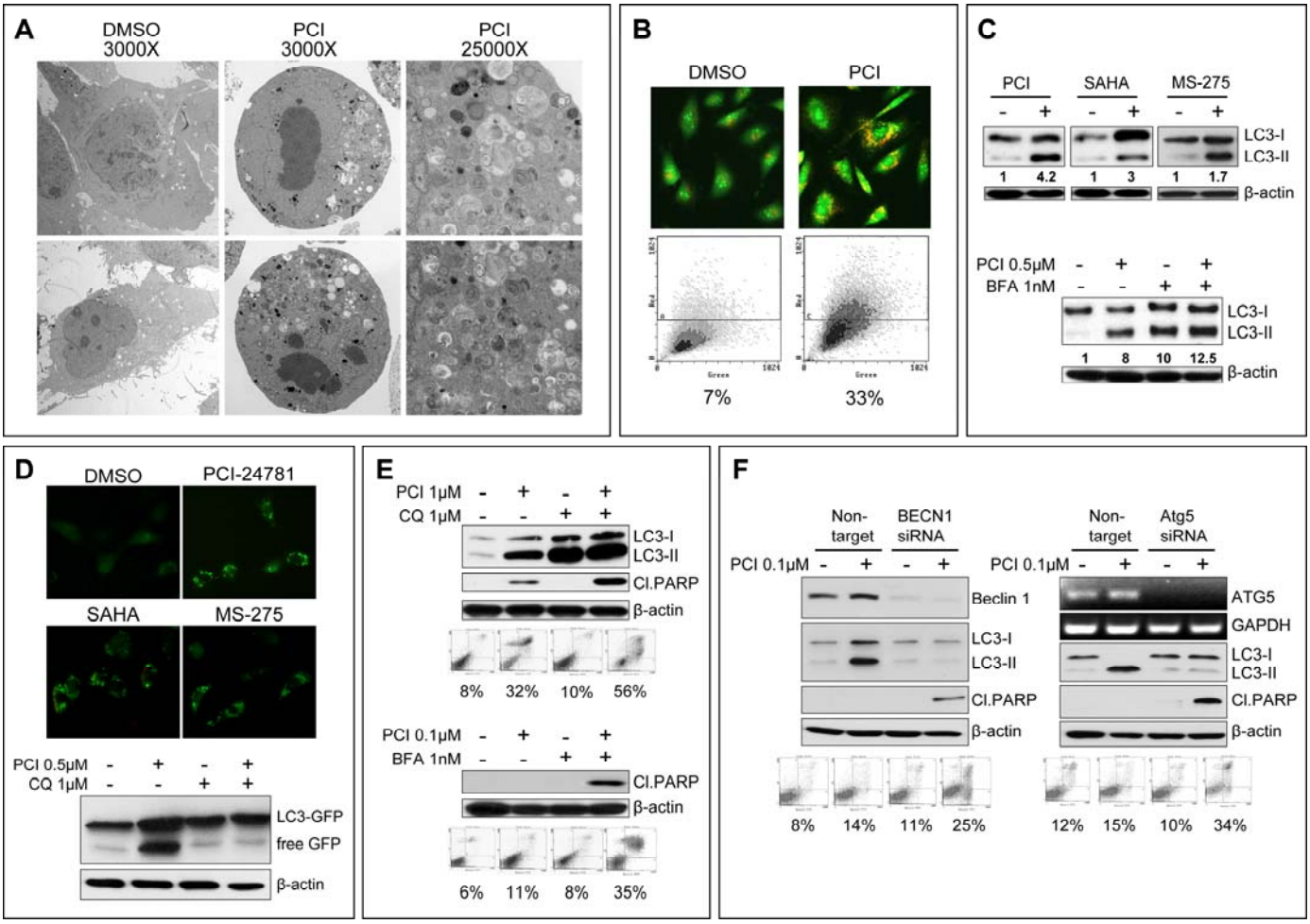

Fig S3: HDACis induce productive autophagy in therapeutic "sensitive" MPNST cells and autophagy blockade further enhances HDACis pro-apoptotic effects in these cells. *A.* TEM pictures demonstrating ultrastructural changes in NF1-associated MPNST cells in response to PCI-24781 (0.5μM/24h). As shown for "resistant" cells (Fig 3A) a large number of autophagic vesicles can be found after HDACi treatment. However, prominent features of apoptosis such as chromatin condensation and loss of nuclear membranes are also evident; *B.* Acridine-orange staining demonstrated increased acidic vesicular organelles (AVOs) in PCI-24781 treated (0.5μM/24hr) NF1-associated MPNST cells (ST88 cells are used as an example) compared to control

DMSO treated cells, as was further confirmed via FACS analysis; *C.* Increased LC3B-II expression (normalized to actin; densitometry values are depicted) was noticed after treatment of “sensitive cells” (S462 is depicted) with any of the HDACis (upper panels; LC3-II expression relative to actin was determined via densitometry). Cells (MPNST642 are depicted as an example) were pretreated (1hr) with low doses of the inhibitors bafilomycin A1 (1nM; shown) or chloroquine (1μM) prior to PCI-24781 treatment (24hr; lower panels). Additional increased LC3B-II expression in response to PCI-24781 treatment was noticed in the presence of these inhibitors; *D.* Cells stably transduced to express LC3-GFP (ST88 are shown as an example) exhibited increased GFP puncta in response to HDACi treatment (upper panels). GFP cleavage was found in response to HDACi and was blocked by pretreatment with chloroquine (lower panels); *E.* Pharmacologic autophagy-inhibition was achieved using chloroquine (upper panel; ST88 cells are depicted as an example) as was confirmed by WB for LC3B-II. PCI-24781 at a dose of 1μM for 24h resulted, as expected, in demonstrable apoptosis in these treatment “sensitive cells”. However, autophagy blockade further increased the apoptotic response as demonstrated by elevated levels of cleaved PARP and Annexin V expression (FACS). Similarly, autophagy blockade using bafilomycin resulted in apoptosis in response to PCI-24781 administered at low dose (0.1μM/24h; lower panel). At this dose significant apoptosis could be seen when PCI-24781 was given alone (T265 cell are shown as an example); *F.* Anti-Beclin siRNA (20nM pool) knockdown in “sensitive” cells (ST88 is shown as an example; left panel) was confirmed via WB and autophagy blockade was validated using LC3B-II WB. Enhanced apoptosis in response to low dose PCI-24781 (0.1μM/24h) was determined via PARP cleavage and Annexin-V/PI FACS analysis. Similar effects were noted after ATG5 knockdown (T265 cells are shown as an example; right panel). Knockdown was confirmed by RTPCR. Together, these experiments demonstrate that HDACis induced autophagy is not exclusive to therapeutic

“resistant” cells but also occurs in “sensitive” MPNST cells albeit in conjuncture with apoptosis. Autophagy induction whether in “sensitive” or “resistant” cells comprises a mechanism of cell survival and autophagy blockade results in enhanced apoptosis.